Journal of
Translational Regenerative Medicine

2026. Volume 1

Research Paper

Rabbit Calvarial Bone Regeneration With Calcium Sulfate, Calcium Phosphate, and Zinc-containing Calcium Phosphate Cements

Saeed Hesaraki[1*], Fatemeh Omidi[2], Davoud Sharifi[2], Javad Ashrafi-Helan[3], Ehsan Fallah[4], Afshin Taheriazam[5]

1. Department of Nanotechnology and Advanced Materials, Materials and Energy Research Center, Karaj, Iran.
2. Department of Clinical Sciences, Surgery and Radiology, Faculty of Veterinary Medicine, University of Tehran, Tehran, Iran.
3. Department of Veterinary Pathology, Faculty of Veterinary Medicine, University of Tabriz, Tabriz, Iran.
4. Department of Orthopedic Surgery, School of Medicine, AJA University of Medical Sciences, Tehran, Iran.
5. Department of Orthopedic Surgery, TeMS.C. Islamic Azad University, Tehran, Iran.

Use your device to scan and read the article online

Citation Hesaraki S, Omidi F, Sharifi D, Ashrafi-Helan J, Fallah E, Taheriazam A. Rabbit Calvarial Bone Regeneration With Calcium Sulfate, Calcium Phosphate, and Zinc-containing Calcium Phosphate Cements. Journal of Translational Regenerative Medicine. 2025; 1:E1020. http://dx.doi.org/10.32598/JTRM.1.1020

http://dx.doi.org/10.32598/JTRM.1.1020

ABSTRACT

Background: Repairing critical-sized calvarial bone defects remains a clinical challenge. Calcium phosphate cement (CPC) is a widely used scaffold, but its properties can be optimized through structural modifications and ionic enrichment. This study aimed to compare the regenerative efficacy of calcium sulfate cement (CSC), macroporous CPC, and zinc sulfate ($ZnSO_4$)-modified macroporous CPC (Zn-CPC) in rabbit calvarial bone regeneration.

Methods: Full-thickness circular defects (10 mm in diameter) were created in the calvaria of 48 adult male New Zealand white rabbits. The Zn-CPC was prepared by incorporating 10 wt% $ZnSO_4$ into the CPC powder. Animals were evaluated at 1, 2, and 3 months post-surgery. Characterization included setting time and compressive strength tests. Bone regeneration was quantified via histomorphometry to calculate trabecular bone volume (BV) fraction.

Results: In-vitro study showed that the use of Zn-CPC reduced the setting time from 12 to 7 minutes and significantly increased compressive strength from about 8 MPa to about 14 MPa. Histological analysis revealed that Zn-CPC supported enhanced osteogenesis compared to CSC and CPC samples. Quantitative histomorphometry demonstrated a progressive increase in new bone formation over the three-month period, with the Zn-CPC group showing the highest trabecular BV fraction and superior integration with the host bone.

Conclusion: The incorporation of $ZnSO_4$ into macroporous CPC not only improves its mechanical properties and setting time, but also significantly enhances its biological performance in vivo. Zn-CPC is a promising candidate for the regeneration of complex craniofacial bone defects.

Keywords: Bone cement, Calcium phosphate, Calcium sulfate, Zinc, Calvarial regeneration

Article info:
Received: 17 Jun 2026
Accepted: 28 Jun 2026
Publish: 03 Aug 2026

*** Corresponding Author:**
Saeed Hesaraki, Professor.
Address: *Department of Nanotechnology and Advanced Materials, Materials and Energy Research Center, Karaj, Iran.*
E-mail: *S-hesaraki@merc.ac.ir*

Highlights

- Calcium sulfate, calcium phosphate, and $ZnSO_4$-containing CPCs were tested for the regeneration of rabbit calvarial bone defects.
- The addition of $ZnSO_4$ improved the setting time and strength of CPCs.
- Zn containing CPCs showed enhanced rabbit calvarial bone regeneration.
- The highest trabecular BV fraction was observed in the Zn-CPC group.

Plain Language Summary

Repairing large and complex bone defects, especially in the skull and face, remains a major clinical challenge because the ideal material must provide both mechanical support and promote new bone formation. In this study, we asked whether adding a small amount of zinc could improve calcium phosphate cement (CPC), since zinc is an essential trace element involved in healthy bone growth and bone-forming cell activity. To address this question, we compared calcium sulfate, macroporous CPC, and zinc sulfate-modified CPC in a rabbit calvarial defect model. The results showed that zinc addition shortened setting time, increased compressive strength, and enhanced new bone formation and integration with the surrounding host bone. Overall, zinc-modified CPC showed superior performance and may be a promising material for craniofacial bone regeneration.

Introduction

Bone tissue possesses a remarkable capacity for self-repair and regeneration. However, this natural healing process is often insufficient when the injury exceeds a "critical size" defect that will not heal spontaneously during the lifetime. Such defects, resulting from high-energy trauma, radical tumor resections, severe infections, or congenital abnormalities, present a monumental challenge to orthopedic and maxillofacial surgeons [1, 2]. The gold standard for treating these defects is the autologous bone graft (autograft), primarily due to its superior osteogenic, osteoinductive, and osteoconductive properties. Nevertheless, autografts are associated with significant limitations, including limited availability, donor-site morbidity, increased surgical time, and potential complications such as chronic pain and infection [3]. To overcome these limitations, bone tissue engineering (BTE) has focused on developing synthetic bone-substitute materials. These scaffolds are designed to serve as temporary templates that support the attachment and growth of osteogenic cells, which are eventually replaced by newly formed host bone [4, 5]. Among the materials investigated, bioceramics, particularly those based on calcium phosphates, have shown the most promise due to their chemical and structural resemblance to the mineral phase of natural bone.

Calcium sulfate cement (CSC), also known as "plaster of Paris", is a widely used bone graft substitute in orthopedic surgery, primarily employed to fill traumatic or surgical bone defects and to serve as a local delivery vehicle for antibiotics in treating infections such as osteomyelitis. Its primary advantages include excellent biocompatibility, osteoconductivity, and the unique ability to be completely resorbed and replaced by host bone over time, all while being relatively cost-effective. However, its clinical application is limited, most notably by its rapid resorption rate (which can sometimes outpace new bone formation) and inherent lack of mechanical strength (which restricts its use in non-load-bearing anatomical sites) [6]. Calcium phosphate cements (CPCs) have emerged as a revolutionary class of bone substitutes since their introduction in the early 1980s [7]. Unlike pre-sintered ceramic blocks, CPCs are composed of powder and liquid phases that, when mixed, form a moldable paste. This paste can be injected into complex-shaped defects or applied via minimally invasive surgical techniques, where it sets in situ to form a solid scaffold typically hydroxyapatite (HA) or brushite [8]. The clinical appeal of CPCs is multifaceted. Beyond their excellent biocompatibility and osteoconductivity, their low-temperature setting reaction allows for the incorporation of heat-sensitive biological molecules or drugs. Furthermore, CPCs are highly bioactive; they form a direct chemical bond with the surrounding bone tissue, minimizing the risk of fibrous encapsulation. Their abil-

ity to be contoured to the specific anatomy of the patient, particularly in delicate areas such as the calvarium (skull) or facial bones, makes them indispensable in reconstructive surgery [9]. Despite their success, first-generation CPCs possess inherent flaws that limit their regenerative potential in large or non-load-bearing defects. One of the most significant issues is the lack of macroporosity. While CPCs are naturally microporous (with pores <10 μm in diameter), they often lack the large, interconnected macropores (>100 μm in diameter) necessary for rapid vascularization and cellular infiltration [10]. Without a vascular network, oxygen and nutrient supply to the implant center is restricted, leading to core necrosis and limited bone ingrowth. Another challenge is the mismatch between the cement degradation rate and the rate of new bone formation. Standard HA-forming CPCs are often too stable in the physiological environment, remaining at the site for years as an inert filler [11]. This prevents the complete restoration of the bone's natural architecture. To address this, research has shifted toward developing porous CPCs using various techniques such as porogen leaching, gas foaming, or 3D printing. Creating a scaffold with an interconnected porous network is essential for facilitating the "creeping substitution" process, in which bone-forming cells and blood vessels gradually replace the synthetic material [12, 13].

To further enhance the biological performance of CPCs, recent strategies have involved doping or modifying the cement matrix with therapeutic ions. Among the essential trace elements, Zinc (Zn) stands out as a potent stimulator of bone formation [14, 15]. Zn is the most abundant intracellular trace element and is highly concentrated in the skeletal system, where it serves as a cofactor for more than 300 enzymes [16]. According to previous studies, Zn ions (Zn^{2+}) exert dual effects on bone metabolism at the cellular level [16, 17]. They significantly promote the proliferation and differentiation of osteoblasts (bone-forming cells) by upregulating osteogenic markers such as alkaline phosphatase (ALP), type I collagen, and osteocalcin. They are also involved in activating the MAPK/ERK signaling pathways, which are crucial for osteogenic gene expression. Zn has been shown to inhibit osteoclasts (bone-resorbing cells), thereby reducing excessive bone turnover and promoting a net gain in bone mass [17]. Furthermore, Zn possesses inherent antibacterial properties, which is a critical advantage in surgical applications where preventing biofilm formation is paramount. However, the concentration of Zn should be carefully controlled. While low concentrations promote healing, excessive levels can lead to cytotoxicity. Therefore, incorporating Zn in a stable form, such as Zn sulfate ($ZnSO_4$), into a CPC matrix enables controlled, localized release that can enhance the microenvironment at the defect site without systemic toxicity [18].

The calvarium, or the skull cap, is a unique anatomical site with specific regenerative requirements. Calvarial bones are often thin and have a limited blood supply compared to long bones, making them more susceptible to non-union fracture. Moreover, the skull's proximity to the brain and its aesthetic importance necessitate a material that is not only biologically active but also mechanically stable and precisely moldable [19]. In this study, we create a porous CPC scaffold modified with $ZnSO_4$. By combining the structural benefits of a macroporous architecture with the biochemical stimulus of Zn ions, we aim to develop a superior bone-substitute material. The main goal of this research is to comprehensively evaluate the efficacy of $ZnSO_4$-modified porous CPC (Zn-CPC) in repairing calvarial bone defects. Through this investigation, we seek to provide a robust scientific basis for the use of zinc-enhanced porous CPCs as a next-generation solution for craniofacial reconstruction and beyond, advancing the goal of rapid, complete functional bone restoration.

Materials and Methods

Materials

In this study, calcium carbonate (Art. No. 102066), calcium hydrogen phosphate anhydrous (Art. No. 102144), zinc sulfate anhydrous (Art. No. 108881), sodium dodecyl sulfate (SDS) (Art. No. 817034), and calcium sulfate hemihydrate (Art. No. 12090) were bought from Sigma-Aldrich Company (Germany). The CSC was prepared by mixing calcium sulfate hemihydrate (powder phase) with distilled water (liquid phase), at a solid-to-liquid ratio of 2 g/mL. The CPC powder consisted of a stoichiometric mixture of dicalcium phosphate anhydrous and tetracalcium phosphate (TTCP). It should be mentioned that TTCP were synthesized by heating an equimolar mixture of calcium hydrogen phosphate anhydrous and calcium carbonate at 1450 for 6 h, followed by quenching to room temperature and grinding to fine powder (10-40 μm). The liquid phase was prepared using a disodium hydrogen phosphate (Na_2HPO_4) aqueous solution containing SDS as a foaming agent to induce porosity within the cement matrix [20]. For the $ZnSO_4$ added group (Zn-CPC), the cement powder was modified by substituting 10% (by weight) of the base CPC powder with $ZnSO_4$. The porous scaffolds were synthesized by mixing the powder and liquid phases at a constant powder-to-liquid (P/L) ratio of 3 g/mL. The

mixture was manually spatulated until a homogeneous paste was formed.

Cement characterization

The initial setting time of the cements was determined in accordance with the American Society for Testing and Materials (ASTM) C266 standard [21]. To prepare the samples, the powder was mixed with the liquid phase (distilled water in the CSC group and SDS-containing sodium hydrogen phosphate solution in the CPC and Zn-CPC groups) at a pre-defined P/L ratio to form a homogeneous paste. The initial setting time was measured using the initial Gillmore needle with a diameter of 2.12 mm and a total mass of 113.4 g. The needle was lowered vertically onto the surface of the specimen at regular time intervals. The initial setting time was defined as the duration from the start of mixing until the needle no longer left a visible indentation (or failed to penetrate the surface) of the cement paste. All measurements were conducted at a constant temperature of 37 ˚C and a relative humidity of 95% to simulate physiological conditions.

The compressive strength of the specimens was evaluated using a universal testing machine (UTM) [22]. To prepare the test samples, the cement paste was poured into cylindrical stainless-steel molds (typically 6 mm in diameter and 12 mm in height). After the samples reached their final setting time, they were removed from the molds and stored in an incubator at 37 ˚C in a physiological buffer solution (phosphate-buffered saline) for 24 hours to ensure complete hydration and mimic the body environment.

The mechanical testing was performed at a crosshead speed of 0.5 mm/min until failure. The maximum load at the point of fracture was recorded, and the compressive strength (σ) was calculated using the following formula: $\sigma=F/A$, where F was the maximum load (N) at failure and A was the cross-sectional area of the specimen (mm^2). The results were reported in Megapascals (MPa) as the mean value of at least five independent measurements per group, presented with the corresponding standard deviation.

The microstructure of the samples was examined using a Stereoscan S360 scanning electron microscope (SEM) at an accelerating voltage of 20 kV and a beam current intensity of 10 nA. Prior to the SEM analysis, the sample surfaces were coated with a thin layer of gold to enhance electrical conductivity and minimize charging effects.

Mercury intrusion porosimetry (Pore Master 60) was employed to evaluate the pore size distribution and total porosity of the samples. Prior to mercury intrusion, the specimens were evacuated to a pressure of 0.5 psi to remove physisorbed gases from the internal pore structure. Measurements were carried out at an equilibration time of 10 s. The applied pressure was progressively increased from 0.5 to 500 psi, then stepwise decreased to atmospheric pressure. Approximately 0.5 g of each sample was analyzed using a 5-cc penetrometer.

In vivo animal study

In this study, 48 adult male New Zealand white rabbits, maintained under standard laboratory conditions, were randomly divided into three equal groups of 6 based on the post-surgery times (1, 2, and 3 months). Prior to surgery, the animals were fasted for 4 hours, with water withheld for 2 hours. Premedication was administered using 2% acepromazine (1 mg/kg). General anesthesia was induced using a combination of ketamine (35 mg/kg), xylazine (5 mg/kg), and diazepam (1 mg/kg). Following the induction of anesthesia, the animals were placed in sternal recumbency. The surgical site (cranial region) was shaved and disinfected using a povidone-iodine (Betadine) scrub and then with an alcohol-Betadine solution. The area was then draped under standard aseptic conditions.

Under general anesthesia, a full-thickness defect (10 mm in diameter) was created in the calvarium using a dental drill (Figure 1). The defects were then filled with the cements, according to the protocols specified in Table 1. Regenerative efficacy and material performance were evaluated with three methods: (i) clinical assessment, including monitoring of physical activity, consciousness level, and local inflammatory signs (e.g. edema); (ii) mechanical testing, where compressive strength was measured using a Zwick/Roell 2005 system at a crosshead speed of 0.01 mm/s; (iii) histopathological analysis, focusing on histomorphological and histomorphometric changes at 30, 60, and 90 days post-surgery.

To prevent potential infections, all rabbits received daily intramuscular injections of penicillin G (60,000 IU/kg) and gentamicin (5 mg/kg) from day 0 to day 5 post-surgery. The surgical sites were inspected daily for clinical signs of complications, including edema, inflammation, wound dehiscence, exudate, or infection.

After the study period, the animals were humanely euthanized in accordance with established veterinary protocols. Initially, sedation was achieved via intramus-

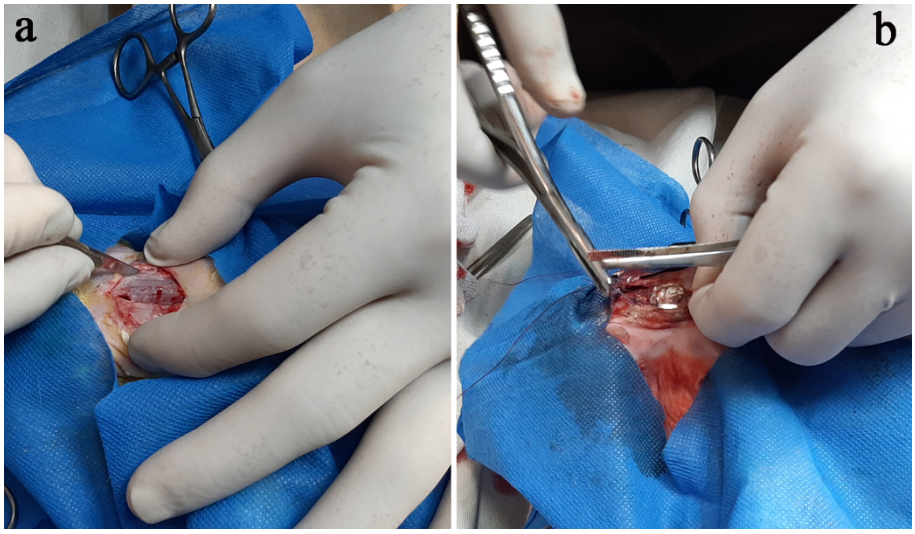

Figure 1. Intraoperative photographs illustrating the surgical procedure on the rabbit calvarium

a) Creation of full-thickness circular defects (10 mm in diameter) using a dental trephine bur under constant irrigation; b) Applying the experimental materials into the defects

cular administration of a ketamine–xylazine mixture, followed by placement of an intravenous catheter. General anesthesia was then induced intravenously (e.g. using propofol or a supplementary anesthetic dose). After confirming the absence of nociceptive reflexes, euthanasia was carried out by intravenous administration of an overdose of a barbiturate such as sodium pentobarbital. Death was verified by confirming the absence of cardiac activity, spontaneous respiration, and corneal reflexes. Then, the surgical sites were re-exposed by incising the skin and reflecting the overlying fascia and musculature. Bone samples containing the implanted materials were carefully harvested from the calvarium, femur, tibia, and mandible. The specimens were immediately immersed in 10% buffered formalin for fixation. Each container was meticulously labeled with the animal's identification details. To preserve tissue architecture and ensure optimal staining quality, a gradual decalcification protocol was employed. After one week of fixation, the samples were transferred to a 5% nitric acid solution supplemented with 1% urea. Due to the use of a lower acid concentration (5% instead of the conventional 10%) to maintain cellular integrity, the decalcification period was extended, lasting 3 weeks for some specimens and up to 2.5 months for denser bones such as the femur. The completion of decalcification was verified using the needle puncture test. Post-decalcification, the samples were returned to 10% buffered formalin before undergoing automated tissue processing, which included dehydration, clearing, and paraffin infiltration. To avoid mechanical artifacts or displacement of the implanted material, each bone specimen was carefully bisected through the center of the implant site using a sharp, new scalpel blade. The specimens were then embedded in paraffin blocks. Longitudinal sections were cut at a thickness of 7µm for bone tissues and 5 µm for parenchymal tissues. The sections were stained with Hematoxylin and Eosin (H&E) according to standard protocols. Histopathological evaluation was performed using an Olympus light microscope to assess biocompatibility, inflammatory response, and bone regeneration.

Quantitative histomorphometric evaluation was performed using Stereo Investigator software, version 9 (MicroBrightField, USA). The BV/TV ratio was estimated using a stereological point-counting method with an M42 test grid based on Cavalieri's principle. Briefly, serial histological sections were prepared and stained according to the study protocol, and the region of interest was consistently defined across all samples prior to analysis. Histological sections were examined under light microscopy, and the grid was superimposed on randomly selected microscopic fields within the region of interest. The number of test points that hit trabecular bone and the total number of points across the entire bone section were recorded. The trabecular bone volume (BV) fraction was then calculated as the ratio of the BV to the total volume (TV) expressed as percentage. To minimize sampling bias, at least five random non-overlapping microscopic fields were evaluated per slide under the same magnification. Fields containing artifacts, torn tissue, or sectioning defects were excluded from analysis. Histomorphometric evaluation was performed by an observer blinded to the experimental groups to reduce measure-

Table 1. Cements used for the treatment of calvarial bone defect in rabbits in the study groups over the study periods

Period (month)	Group A	Group B	Group C	Group D
1	Control	Porous CPC	CSC	Porous CPC + Zn
2	Control	Porous CPC	CSC	Porous CPC + Zn
3	Control	Porous CPC	CSC	Porous CPC + Zn

ment bias, and the mean value for each specimen was used for statistical analysis.

Statistical analysis

Statistical analysis was performed in IBM SPSS software, version 26, R software, version 4.3.1, and GraphPad Prism software, version 9. Descriptive statistics were used to report data; Mean±SD for continuous variables and percentages for categorical data. To compare groups, an independent t-test and chi-square test were employed. Normality was assessed using the Shapiro-Wilk test. In all analyses, $P<0.01$ was considered statistically significant.

Results

Setting time and compressive strength

Figure 2 illustrates the setting time and compressive strength of three cement samples. The minimum setting time belonged to the CSC sample. The incorporation of $ZnSO_4$ significantly accelerated the setting process of the cement. The CPC sample showed a setting time of approximately 12 minutes, whereas the Zn-CPC sample exhibited a reduced setting time of approximately 7 minutes. This suggests that $ZnSO_4$ acts as an effective setting accelerator for the CPC matrix.

The CPC and CSC samples exhibited comparable compressive strength. The addition of $ZnSO_4$ led to a notable improvement in the mechanical properties of the CPC. The CPC sample showed a compressive strength of approximately 8 MPa. In contrast, the CPC, combined with $ZnSO_4$, exhibited a significantly higher compres-

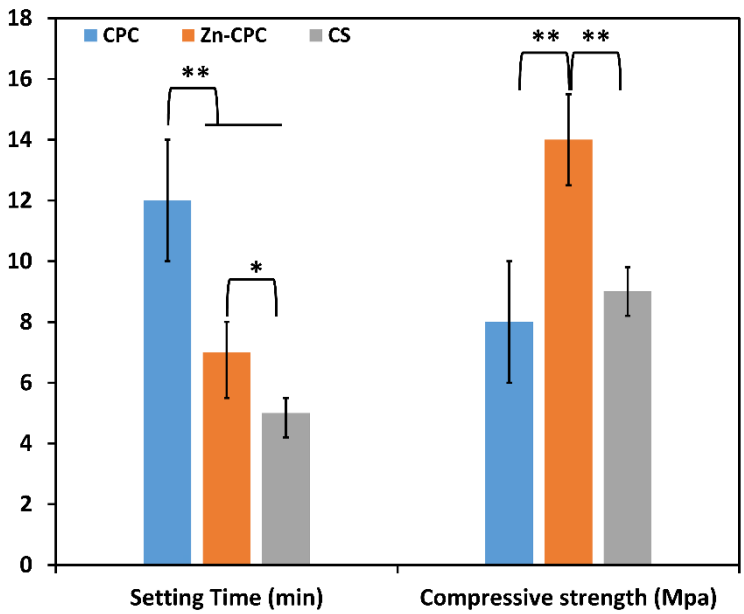

Figure 2. The setting time and compressive strength of the CSC, CPC and Zn-CPC samples

*P<0.01, **P<0.05.

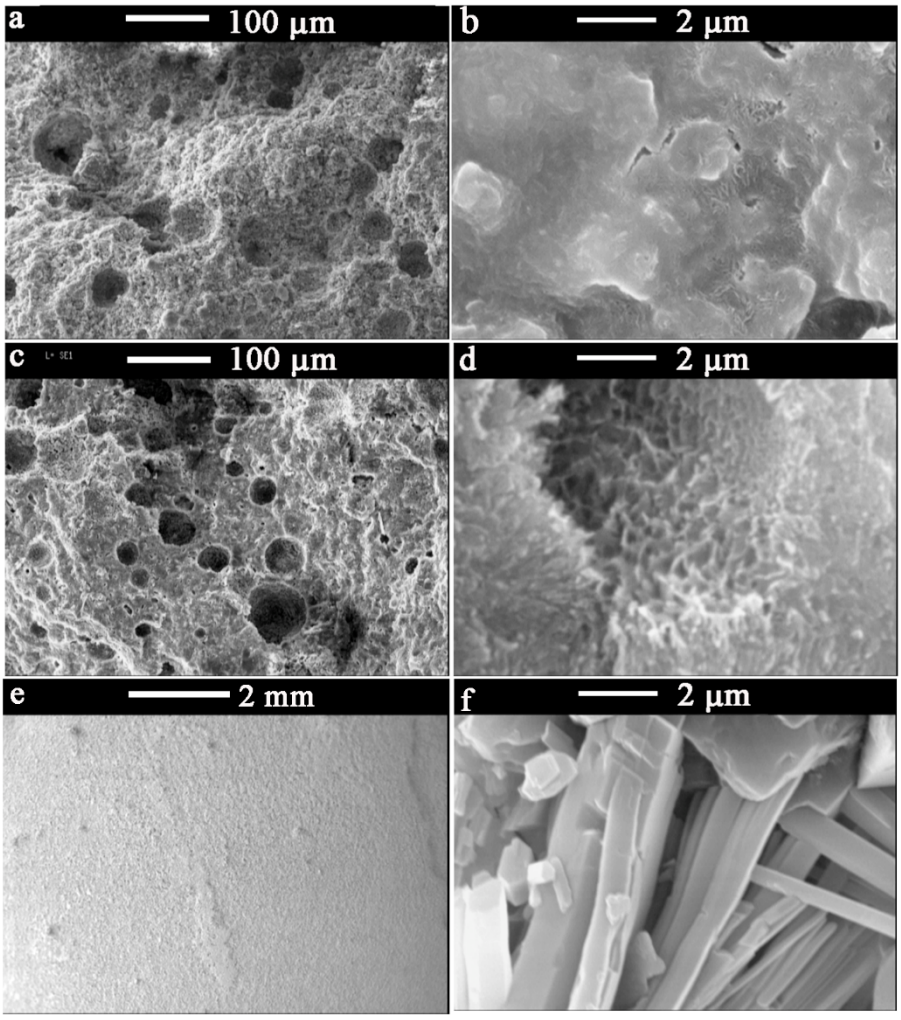

Figure 3. The SEM images of CPC (a and b), Zn-CPC (c and d), and CSC (e and f) samples

sive strength of approximately 14 MPa. This indicates that the inclusion of $ZnSO_4$ contributes to a stronger, more robust mechanical structure.

Based on the results, it can be said that CPC with $ZnSO_4$ provides a dual benefit; it accelerates the setting time (increasing processing efficiency) and substantially enhances the compressive strength (improving structural integrity). These trends were consistent across the prepared samples.

Microstructure

Figure 3 shows the SEM micrographs of three cement samples. As can be seen, both CPC and Zn-CPC samples exhibited macroporosity, characterized by numerous circular to irregularly shaped voids (Figures 3a and 3c). These pores were distributed throughout the material. The pure CPC sample seems to have a slightly higher density of smaller pores or a more intricate pore network compared to the Zn-CPC sample. The images indicated that these pores were in the range of 10-100 µm. The images at higher magnification (Figures 3b and 3d) revealed finer details of the cements' surfaces and microstructures. In Figures 3b, the surface of the porous CPC showed a relatively smooth, possibly aggregated structure with some finer crystal features. The texture suggests a degree of micro-level heterogeneity. Porous Zn-CPC revealed a more distinct and intricate morphology. The surface is covered with needle-like or plate-like crystalline structures. These crystals appear to be growing within the cement matrix, indicating a potential change in the material phase composition due to the addition of $ZnSO_4$. The orientation and density of these crystals suggest a specific growth pattern. Overall, the SEM images showed that adding $ZnSO_4$ to the porous CPC alters its microscale surface morphology. While both materials are highly porous, the Zn-CPC exhibits

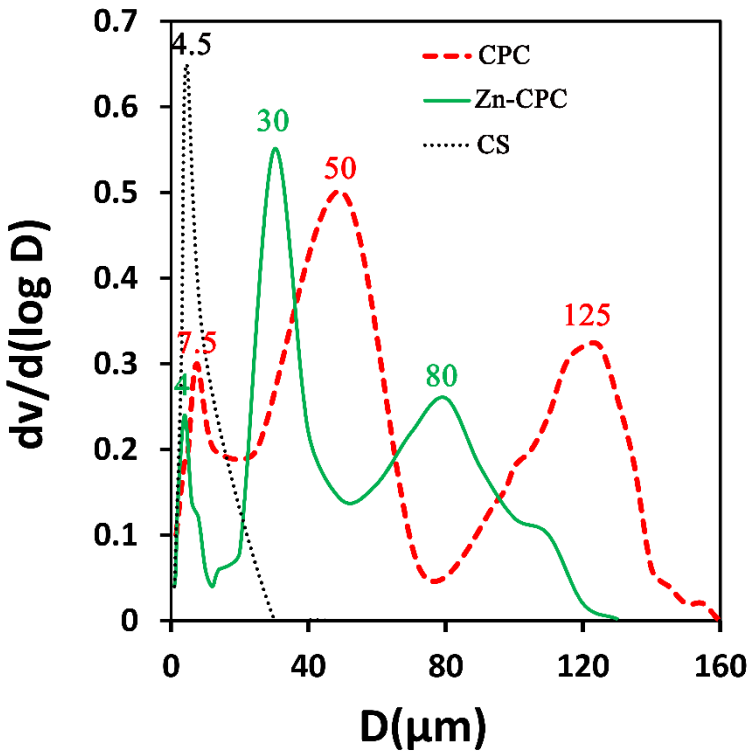

Figure 4. The pore size distribution in the CSC, CPC and Zn-CPC samples

a more pronounced crystalline, acicular/plate-like structure, suggesting a different phase or depositional process than the CPC.

Figure 3e and 3f illustrates the hierarchical microstructure of CSC at two different scales. At low magnification (2 mm), the surface appears as a dense yet granular matrix with evident microporosity. In contrast, the high-magnification image (2 μm) reveals the distinct morphology of the crystals, characterized by an elongated, columnar, and plate-like structure. These crystals form an intricately interlocking network, which is responsible for the cement's mechanical setting. This porous, crystalline arrangement facilitates fluid transport and provides a high surface area, supporting the material's rapid bioresorption and integration with host bone tissue.

Pore size distribution

Figure 4 shows the pore size distribution for the CSC, CPC and Zn-CPC samples. In the CSC, a monomodal pore size distribution was observed in which micropores concentrated at about 4.5 μm. The two other graphs display a multimodal distribution for both CPC and Zn-CPC samples, indicating that the porosity is concentrated in several distinct size ranges rather than a single uniform size. Pure CPC showed three primary peaks at approximately 7.5, 50, and 125 μm. The highest volume of pores was concentrated in the mid-to-large range (125 μm). In Zn-CPC, the peaks were shifted toward smaller diameters, located at 4 μm, 30 μm, and 80 μm. The most prominent peak occured at 30 μm, indicating a significant refinement of the pore structure. Comparing the two samples revealed several key impacts of adding $ZnSO_4$. The entire distribution shifts to the left. This indicates that the addition of $ZnSO_4$ leads to a finer porous structure, reducing the overall size of the voids within the cement matrix. The large pores observed in the pure CPC (around 125 μm) were significantly reduced in the zinc-containing sample, with the largest significant peak dropping to 80 μm. There was a much higher concentration of pores in the 30 μm range compared to the pure sample, suggesting a more compact and interconnected microporous network. In CPC, micropores were formed by the spaces between precipitating crystals (usually HA). Zinc ions are known to act as crystal growth inhibitors. By preventing the growth of large crystals, zinc promotes the formation of many smaller crystals, which naturally results in smaller inter-crystalline spaces (pores). Generally, a shift toward smaller pore sizes (pore refinement)

is associated with an increase in compressive strength, as shown in Figure 2. Large macropores (>100 µm) often act as stress concentrators; therefore, the reduction of the 125 µm peak in the zinc-containing sample may improve the mechanical integrity of the cement. From a biological perspective, micropores <10 µm are crucial for the circulation of body fluids and the transport of nutrients and proteins. All samples remained within this range. The presence of macropores (>100 µm) is typically required for bone ingrowth (osteoconduction) and blood vessel formation (angiogenesis). Although the Zn-CPC sample had fewer macropores, the high frequency of pores at 30 µm and 80 µm can allow for significant biological activity. In CSC, in addition to the lack of macropores, the rapid in vivo dissolution and resorption can create a dynamic, interconnected porosity that allows for the simultaneous ingrowth of blood vessels and osteogenic cells, effectively transforming the dense material into a transient scaffold that supports new bone formation through a process known as "creeping substitution." Beyond structural changes, Zn is an essential trace element that stimulates osteoblast (bone-forming cell) activity and provides antibacterial properties.

The results indicated that $ZnSO_4$ acts as a structural modifier in CPC. It effectively refines the pore diameter, shifting the dominant pore size from 50 µm to 30 µm and reducing large macropores. This likely result in a stronger, denser cement with modified bioresorption rates and added therapeutic benefits from the Zn ions.

In vivo findings

Clinical observations

Highly effective and standardized anesthetic protocol was employed for all rabbits in both experimental groups to ensure a uniform surgical procedure. The administration of a combined acepromazine/ketamine/diazepam provided optimal anesthesia and profound analgesia. This protocol successfully allowed for skin incision and the creation of the cranial defect without any physical reflexive reactions throughout the 20-min surgical duration. The animals regained full physical activity 125 minutes after the induction of anesthesia. All animals resumed normal water and food consumption within 24 hours post-surgery. No specific or unexpected clinical complications were observed in any animals throughout the study period. Skin sutures were removed on the 12th postoperative day. Upon clinical inspection, tissue adhesion was observed between the cement and the overlying skin in all rabbits, indicating a stable interface. Over time, the implanted cement transitioned to a pale yellow hue at the defect site. Furthermore, the material demonstrated successful integration with the surrounding host bone tissue, maintaining a relatively smooth surface profile.

Histopathological outcomes

Figure 5 shows histopathological images of the defect site one month after implantation in the study groups. Based on the histopathological findings, the absence of significant inflammatory reactions (such as infiltration of giant cells, lymphocytes, or neutrophils) in all experimental groups is crucial. It confirms that the CSC, CPC, and the Zn-CPC were highly biocompatible and did not trigger a detrimental immune response, which is a prerequisite for bone substitute materials. In group A (control group free of filler), the defect was filled mainly with granulation tissue, and no bone formation was observed. No significant inflammatory reaction was detected. In group B (CPC group), the defect area was predominantly filled with calcium phosphate deposits, with a small amount of granulation tissue formation. Limited osteoid deposition was observed, but no bone formation was seen, and no significant inflammatory response was present. After one month, the material persisted in the defect. While it provides a space-filling effect, the limited osteoid suggests that the material may be degrading slowly or lack the osteoinductive signals to promote rapid bone maturation on its own. In group C (CSC group), the defect was filled with granulation connective tissue, and a considerable amount of calcium deposition occurred. Osteoid deposition was also visible. In one region adjacent to the intact cortical bone, some cartilaginous tissue had formed within the granulation tissue, but no bone tissue was observed. In group D (Zn-CPC group), calcium phosphate deposits and granulation connective tissue were observed, and the thickness of collagen fibers was greater than in other groups. Osteoid deposition was present, and no significant inflammatory reaction was observed. The combination of CPC with $ZnSO_4$ appears to create a more favorable environment. The observation of "thicker collagen fibers" was notable. Collagen architecture is the precursor to a strong mineralized matrix. This suggests that the composite promotes a more organized organic matrix, which is necessary before mature bone mineralization can occur. Overall, at one month, the primary presence of granulation tissue and osteoid (unmineralized bone matrix) across all groups indicates that the defect is in an active regenerative phase. It is normal at this stage not to see fully formed, mature, mineralized lamellar bone in a critical-sized defect. The key success factor here is the quality of the precursor tissues

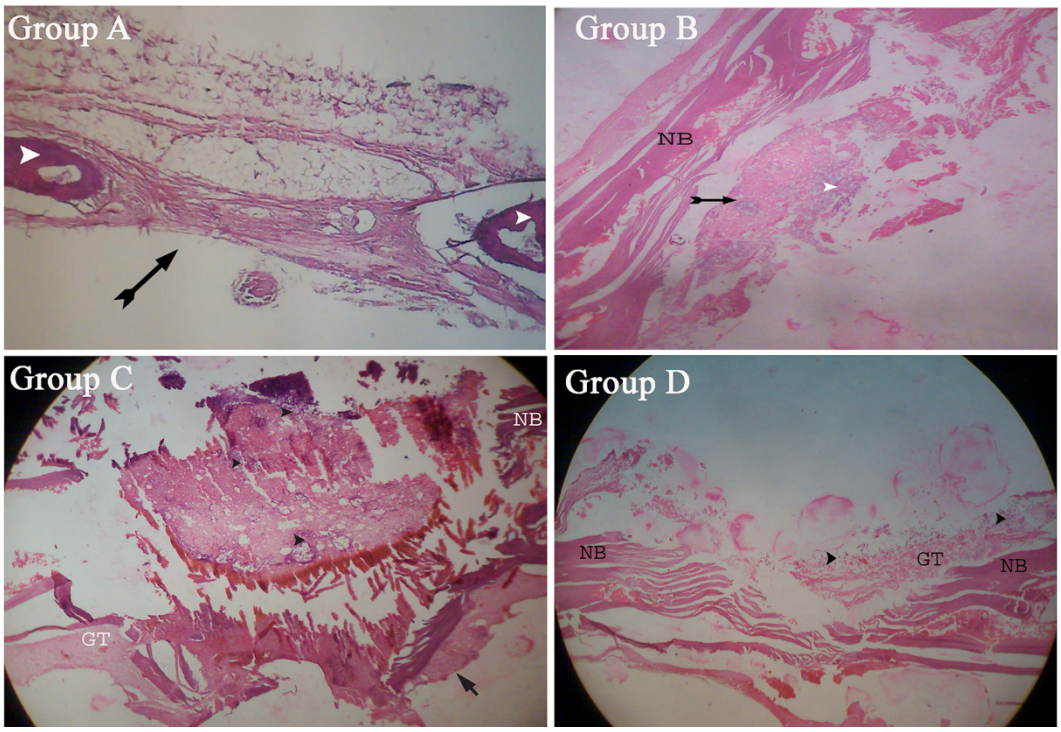

Figure 5. Histopathological images of cranial bone defects in rabbits one month post-surgery, filled with different cements (H&E staining at ×64 magnification)

Group A: Control, filled with granulation tissue (GT) shown by the arrow. In this group, normal bone (NB) was visible (shown by the arrowhead); Group B) CPC group, which includes a section of NB, GT (arrow), and calcium phosphate deposits (arrowhead); Group C) CSC group, filled with calcium phosphate deposits (arrowhead) and GT: in this group, newly formed cartilaginous tissue (arrow) can be seen in the lower part of the image; Group D: Zn-CPC group, where near the NB, the defect is filled with calcium phosphate deposits (arrowhead) and GT containing relatively thick collagen fibers.

(collagen density and presence of osteoid), which appears superior in group D.

Figure 6 shows histopathological images of the cranial bone defects three months post-surgery. In the control group, the defect was partially filled with granulation tissue characterized by thick collagen fibers. Significant areas of newly formed bone, exhibiting both medullary and cortical structures containing osteocytes, were also observed. In the CPC group (group B), the defect was almost completely occupied by newly formed bone (both cortical and medullary) containing osteocytes. The calcium deposits were entirely resorbed. However, some granulation tissue persisted around the defect periphery, and bone remodeling was not yet complete. In the CSC group (group C), granulation tissue occupied the defect site. Medullary bone formation also occurred but remained incomplete. Osteocytes were visible within the new bone matrix, and islands of cartilaginous tissue were present between the newly formed bone structures. In the Zn-CPC group (group D), the defect was largely filled with newly formed bone. Bone formation initiated in the medullary region and progressed toward the cortex. One side showed a fully formed cortex, while the other side still contained residual granulation tissue. Calcium deposits were completely resorbed.

Figure 7 presents the results of quantitative analysis of bone regeneration. Data were expressed as the trabecular BV fraction within the defect area. It revealed a progressive increase in bone formation across all groups over the 3-month period. In the first month, the control group (group A) exhibited the lowest percentage (15.75±5.23%), while all treated groups showed significantly higher BV fraction, with the CPC group (Group B) and the Zn-CPC group (group D) reaching 26.13±4.98% and 25.36±5.12%, respectively. The CSC group (group C) showed a similar regenerative pace at 23.35±7.56%. In the second month, a significant acceleration in bone maturation was observed, particularly in group D, which reached 39.23±3.26%, outperforming groups B and C. The control group remained significantly lower at 23.32±4.15%. In the final follow-up period (3 months), group D demonstrated the highest regenerative capacity, with a trabecular BV fraction of 58.23±9.12%, followed by groups C and B, both of which showed

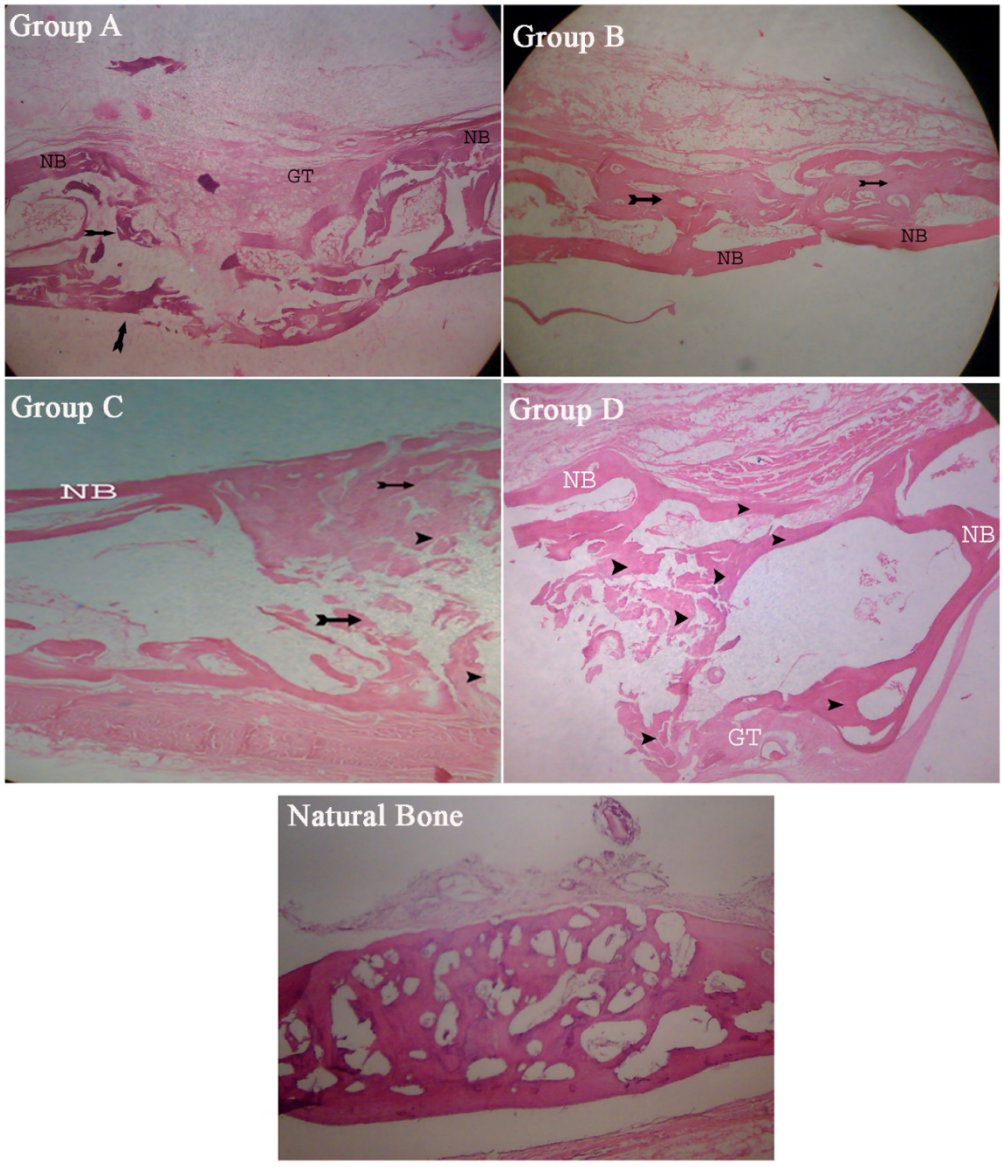

Figure 6. Histopathological images of cranial bone defects in rabbits filled with various cements three months post-surgery (H&E staining at ×64 magnification)

Group A) Control group, filled with granulation tissue (GT) along with the formation of new bone (NB) shown by the arrows; Group B) CPC group, where newly formed bone tissue (arrow) fills the defect site, and GT is visible above the new bone; Group C) CSC group, in which the defect exhibits GT (arrowhead) along with newly formed bone structures (arrow); Group D) Zn-CPC group, in which bone tissue (arrowhead) almost completely fills the defect: some residual GT remains, showing the active transition of fibroblasts into osteocytes.

Note: The image of natural bone (lower image) is provided as a histological reference of mature, healthy bone architecture.

nearly double the BV fraction compared to the control group ($P<0.01$). Overall, a significant progressive trend in bone formation was observed in group D, where the trabecular BV fraction increased from 25.36% in the first month to 58.23% in the third month ($P<0.05$).

In the third month post-surgery, the complete resorption of calcium phosphate deposits in groups B and D was notable. This indicates that the cements had a suitable degradation rate that matches the pace of new bone ingrowth. The transition from "osteoid" (seen in the first month) to cortical and medullary bone containing osteocytes (in the third month) showed that the materials were osteoconductive. Hence, Zn-CPC showed a more advanced stage of maturation compared to pure CPC, suggesting that the combination of the CPC scaffold and

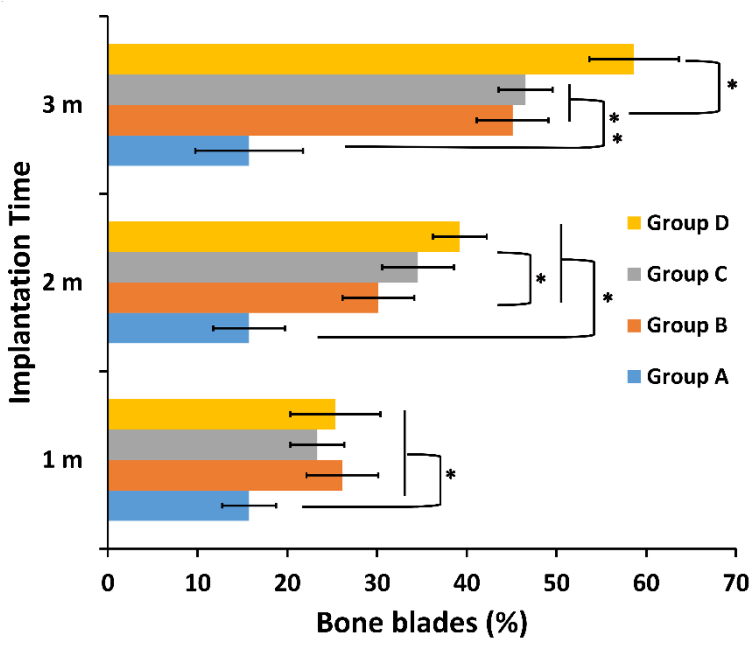

Figure 7. Trabecular BV fractions in the study groups at three post-surgery times

*P<0.01, **P<0.05.

the Zn additive synergistically promotes the transition from medullary to cortical bone. Although, in group C (CSC group), the presence of cartilaginous tissue persisted even over 3 months, and bone formation was medullary but incomplete, in group D (CPC + Zn), the healing was more organized. This suggests that while Zn influences the biological pathway (as seen by the cartilage formation); it requires the structural scaffold of the CPC to effectively guide bone formation toward a complete cortical structure. The fact that remodeling is incomplete in all groups 3 months post-surgery was expected for cranial defects in rabbits. However, the presence of thick collagen fibers in group A and the advanced cortical progression in group D was a positive indicator of the long-term mechanical stability of the regenerated site.

Overall, the 3-month post-surgery results demonstrated a clear progression in bone healing compared to the 1-month stage. Specifically, group D showed the most advanced regeneration, where the transition from fibrous granulation tissue to mineralized bone matrix (osteocytes) was nearly complete. The presence of natural bone in the images can serve as a benchmark to show how closely the newly formed bone in the experimental groups mimics the original cortical and medullary structure.

Biomechanical evaluation

The mechanical properties and fracture load of the regenerated bone at the implant sites were characterized using a Zwick/Roell Z005 universal testing machine. To evaluate the regenerative efficacy of different materials implanted in the rabbit calvaria, mechanical strength and Young's modulus of elasticity were determined based on the recorded force-displacement and stress-strain curves. The fracture limit, defined as the peak force at which structural failure or rupture of the bone-material complex occurs, was measured for each sample. All tests were conducted at a constant crosshead speed of 0.01 mm/s to ensure quasi-static loading conditions.

Figure 8 illustrates the compressive load (mechanical strength) of bone defects over a three-month period in different groups, including normal bone, unfilled bone defects (group A), bone defects filled with porous CPC (group B), bone defects filled with CSC (group C), and bone defects filled with a combination of porous CPC and $ZnSO_4$ (group D). Overall, all experimental groups showed a progressive increase in mechanical strength from the first month to the third month. This suggests a time-dependent healing process and gradual integration of the filling materials with the host bone. Normal bone maintained a stable and high mechanical strength, ranging from 249±4 N to 255±4 throughout the study, serving as the benchmark for full recovery. The unfilled

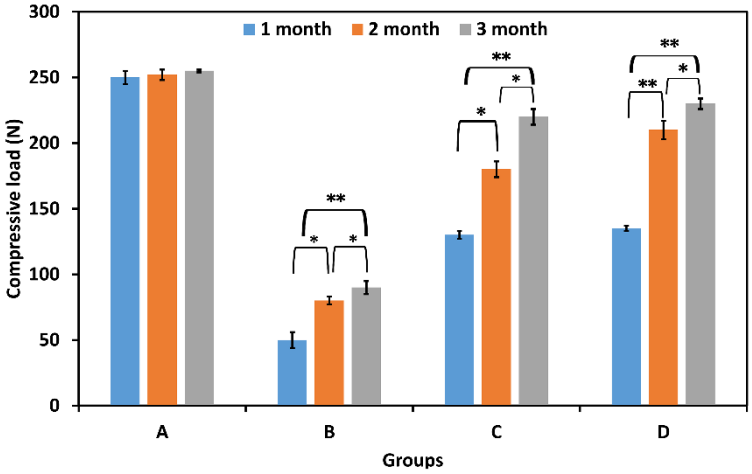

Sample	Group	1 Month	2 Months	3 Months
Normal Bone	-	249 ± 4	250 ± 3	255 ± 4
Unfilled	A	51±14	80 ± 19	95 ± 4
CPC	B	128 ± 20	188 ±10	213 ± 5 6
CS	C	84 ± 12	152 ± 14	185 ± 8
Zn-CPC	D	132 ± 18	210 ± 12	235 ± 10

Figure 8. The compressive fracture load of various samples at different post-surgery periods

*P<0.01, **P<0.05.

bone defect (group A) exhibited the lowest mechanical strength in all time points (51±14 at month 1 to 95±4 N at month 3), indicating that without filling materials, the natural healing process is significantly slower and less effective in restoring structural integrity. The bones filled with CPC (group B) and CSC (group C) showed significant improvement in the compressive load compared to the unfilled bones. Group B reached 213±56 N by the third month, while group C reached 185±8 N. In group D, the combination of porous CPC and $ZnSO_4$ demonstrated the best performance among the experimental groups. By the third month, it reached a compressive load of 235±10 N, which is the closest value to the strength of normal bone (255 N). The results indicate a clear synergistic effect when $ZnSO_4$ is added to porous CPC. Group D consistently outperformed groups B and C at all post-surgery times, especially at the third month, which achieved approximately 92% of the mechanical strength of a normal bone.

Discussion

The setting time and mechanical performance of CPCs are critical factors for determining their clinical applicability, particularly in repairing craniofacial and calvarial bone defects. In the present study, 10 wt.% of $ZnSO_4$ was added to CPC powder to formulate the Zn-CPC sample. The selection of 10 wt% $ZnSO_4$ was based on previous optimization studies. Several concentrations of $ZnSO_4$ were evaluated, and it was observed that increasing the $ZnSO_4$ content above 10 wt% significantly accelerated the setting process, resulting in poor workability and reduced handling time. In contrast, lower concentrations were associated with insufficient Zn release in the surrounding medium. Therefore, 10 wt% $ZnSO_4$ was selected as an optimal compromise between cement processability, setting behavior, and biologically relevant Zn release. This concentration was chosen to maintain practical usability while providing a Zn-modified formulation with potential benefits for bone regeneration applications.

The incorporation of $ZnSO_4$ into the CPC reduced the setting time and improved mechanical strength, indicating that $ZnSO_4$ positively influenced both the physicochemical and structural characteristics of the cement. The reduction in the setting time of the cement following the addition of $ZnSO_4$ can be attributed to the presence of sulfate ions, which play an important role in modifying the ionic environment during the early stages of

cement hydration. The sulfate ions increase the overall ionic strength and supersaturation of the liquid phase with respect to the forming calcium phosphate or even sulfate minerals. This elevated supersaturation creates more favorable conditions for rapid nucleation of ion-substituted apatite crystals, thereby accelerating the transition from a viscous paste to a hardened solid matrix. As a result, the CPC sets faster, reducing the window during which the material is susceptible to mechanical disturbance or washout after implantation. Importantly, this accelerated setting process remains within clinically acceptable limits, preserving the handling properties necessary for precise placement during surgery.

Along with the reduced setting time, $ZnSO_4$ incorporation enhanced the mechanical strength of the CPC scaffold. This improvement is likely influenced by changes in the microstructural organization of the cement. The combined presence of Zn and sulfate ions may lead to the formation of a more tightly interlocked and homogeneous crystal network (as shown in the cement microstructure), with fewer microdefects or voids within the matrix. These mechanical improvements are significant because conventional CPCs are often limited by their inherent brittleness and relatively low strength, especially when macroporosity is introduced to support vascularization and cellular infiltration. The strengthening effect associated with $ZnSO_4$ helps mitigate this trade-off by reinforcing the structural integrity of the scaffold while still preserving its biologically necessary porosity. Enhanced mechanical strength also contributes to improved graft-host integration by providing early structural support for cellular attachment and extracellular matrix deposition. Additionally, the improved setting and mechanical properties may synergistically contribute to the superior biological outcomes observed with Zn-modified CPCs. Faster hardening and greater initial strength create a more stable microenvironment at the bone–cement interface, supporting early osteoblastic activity and facilitating the increased collagen type I synthesis and alkaline phosphatase expression documented in the study. These combined physicochemical and biological effects reinforce the potential of Zn-CPC as a multifunctional bone graft substitute. The results also demonstrated that the incorporation of $ZnSO_4$ into porous CPC significantly enhanced its osteogenic potential, overcoming the limitations of conventional CPC scaffolds. These findings indicate that the controlled release of Zn ions from the porous matrix acts as a potent biochemical stimulus, modulating both the cellular behavior of osteoblasts and the structural integrity of the newly formed bone tissue.

A critical observation in this study was the dual role played by Zn ions. Consistent with recent advancements in BTE, our data confirmed that Zn ions stimulate the proliferation and differentiation of osteoblasts, as evidenced by the elevated expression of alkaline phosphatase and increased Type I Collagen synthesis observed in our in vivo calvarial bone defect models of rabbits. Furthermore, the localized release of Zn appears to exert an inhibitory effect on osteoclast activity. This dual role (promoting bone formation while simultaneously inhibiting bone resorption) is essential for achieving rapid and high-quality bone regeneration in critical-sized defects. The superiority of our Zn-CPC composite over conventional CPCs is evident with respect to the BV/TV ratio. While standard CPC provides a biocompatible, osteoconductive scaffold, it often lacks the bioactivity required to bridge large gaps efficiently. The introduced macroporosity in the CPC scaffold combined with the biochemical signaling of the Zn dopant, facilitated enhanced cellular infiltration and vascularization within the bone defect site. This interconnected porous architecture, coupled with the chemical presence of Zn, allowed for a more harmonious integration between the graft material and the host tissue, leading to a stronger and denser mineralized interface than that observed in the control groups. Consistent with a similar study [23], the results underscores the superior performance of Zn-containing cements over conventional, unmodified CPC formulations. Previous studies have consistently shown that while pure CPC provides a stable osteoconductive framework, it often lacks the necessary signals to trigger rapid biological responses. In contrast, similar investigations on trace element doping in bioceramics such the study by Li et al. [24] have shown that the addition of Zn leads to significantly higher BV/TV ratio and enhanced interfacial bonding in animal models. Furthermore, our findings are consistent with the results of studies reported that Zn-incorporated grafts exhibit superior osteoinductive-like properties compared to strontium or magnesium-doped scaffolds in certain craniofacial applications. These observations suggest that the controlled release of Zn from the CPC and $ZnSO_4$ composite acts as a potent catalyst for bone remodeling, establishing it as a promising candidate for advanced maxillofacial bone engineering.

The success of applying the prepared scaffold in the rabbit model highlights the significance of the release kinetics of Zn. By adding a concentration of $ZnSO_4$ into the CPC matrix, we may achieve a release that remain within the therapeutic window avoiding the potential cytotoxicity associated with high systemic Zn levels. This release is a primary factor in the accelerated mineraliza-

tion and superior mechanical interlock observed at the defect margins. Despite these promising results, several aspects warrant further investigation. While the short-term outcomes in the rabbit model were compelling, the long-term degradation rate of the Zn-doped CPC in relation to the rate of new bone formation remains to be fully investigated. Additionally, while we have identified the osteogenic benefits, the precise intracellular signaling pathways triggered by the Zn ions in this specific CPC formulation deserve deeper molecular exploration to further refine the materials composition.

Conclusion

The findings of this study demonstrate that the addition of $ZnSO_4$ can significantly improve the physicochemical and biological performance of porous CPCs. It can reduce the setting time from approximately 12 minutes to about 7 minutes and increase the compressive strength from nearly 8 MPa to around 14 MPa, indicating enhanced handling characteristics and mechanical stability. The porous structure of the scaffold provides a favorable environment for tissue ingrowth and bone regeneration. The in vivo study on rabbits' calvarial bone defects showed progressive bone healing over the experimental periods of 1, 2, and 3 months. Histopathological observations revealed improved tissue integration and greater new bone formation in defects filled with Zn-CPC compared to those with CSC and porous CPC. These results suggest that the presence of Zn ions may promote osteogenic activity and enhance the regenerative capacity of the scaffold. Overall, porous Zn-CPC has a promising potential as a bone substitute material for the repair of calvarial bone defects. Its higher mechanical properties, suitable setting behavior, and favorable biological response indicate make it a useful candidate for future applications in BTE and regenerative medicine. Further studies with longer observation periods and larger sample sizes are recommended to confirm its clinical applicability.

Ethical Considerations

Compliance with ethical guidelines

All experimental procedures involving animals were conducted in compliance with institutional ethical standards and animal care regulations. This study was approved by the Research Ethics Committee of the AJA University of Medical Sciences, Tehran, Iran (Code: IR.AJAUMS.REC.1402.127).

Funding

This research was funded by the Materials and Energy Research Center and the Faculty of Veterinary Medicine, University of Tehran, Tehran, Iran (Grant No.: 14043037).

Authors' contributions

Conceptualization and writing of the initial and final drafts: Saeed Hesaraki; Methodology and investigation: Saeed Hesaraki and Fatemeh Omidi; Data analysis: Ehsan Fallah and Afshin Taheriazam; Project administration: Davoud Sharifi.

Conflict of interest

The authors declared no conflict of interest.

Acknowledgments

The authors would like to thank Morteza Mehrjoo for his valuable assistance in conducting this research. The authors also acknowledge Sadra Modern Arya Company for their support.

References

[1] Bauer TW, Muschler GF. Bone graft materials: An overview of the basic science. Clinical Orthopaedics and Related Research. 2000; (371):10-27. [DOI:10.1097/00003086-200002000-00003] [PMID]

[2] Shahrezaie M, Zamanian A, Sahranavard M, Shahrezaee MH. A critical review on the 3D bioprinting in large bone defects regeneration. Bioprinting. 2024; 37:e00327. [DOI:10.1016/j.bprint.2023.e00327]

[3] Baldwin P, Li DJ, Auston DA, Mir HS, Yoon RS, Koval KJ. Autograft, allograft, and bone graft substitutes: clinical evidence and indications for use in the setting of orthopaedic trauma surgery. Journal of Orthopaedic Trauma 2019; 33(4):203-13. [DOI:10.1097/BOT.0000000000001420] [PMID]

[4] Schieker M, Seitz H, Drosse I, Seitz S, Mutschler W. Biomaterials as scaffold for bone tissue engineering. European Journal of Trauma. 2006; 32(2):114-24. [DOI:10.1007/s00068-006-6047-8]

[5] Hesaraki S, Saba G, Shahrezaee M, Nezafati N, Orshesh Z, Roshanfar F, et al. Reinforcing β-tricalcium phosphate scaffolds for potential applications in bone tissue engineering: Impact of functionalized multi-walled carbon nanotubes. Scientific Reports. 2024; 14(1):19055. [DOI:10.1038/s41598-024-68419-2] [PMID]

[6] Borhan S, Hesaraki S, Ahmadzadeh-Asl S. Evaluation of colloidal silica suspension as efficient additive for improving physicochemical and in vitro biological properties of calcium sulfate-based nanocomposite bone cement. Journal of Materials Science: Materials in Medicine. 2010; 21(12):3171-81. [DOI:10.1007/s10856-010-4168-4] [PMID]

[7] Chow LC. Development of self-setting calcium phosphate cements. Journal of The Ceramic Society of Japan. 1991; 99(1154):954-64. [DOI:10.2109/jcersj.99.954]

[8] Yousefi AM. A review of calcium phosphate cements and acrylic bone cements as injectable materials for bone repair and implant fixation. Journal of Applied Biomaterials & Functional Materials. 2019; 17(4):2280800019872594. [DOI:10.1177/2280800019872594] [PMID]

[9] Heinemann S, Rössler S, Lemm M, Ruhnow M, Nies B. Properties of injectable ready-to-use calcium phosphate cement based on water-immiscible liquid. Acta Biomaterialia. 2013; 9(4):6199-207. [DOI:10.1016/j.actbio.2012.12.017] [PMID]

[10] Lodoso-Torrecilla I, van Gestel NAP, Diaz-Gomez L, Grosfeld EC, Laperre K, Wolke JGC, et al. Multimodal pore formation in calcium phosphate cements. Journal of Biomedical Materials Research Part A. 2018; 106(2):500-9. [DOI:10.1002/jbm.a.36245] [PMID]

[11] Lee K, Weir MD, Lippens E, Mehta M, Wang P, Duda GN, et al. Bone regeneration via novel macroporous CPC scaffolds in critical-sized cranial defects in rats. Dental Materials. 2014; 30(7):e199-207. [DOI:10.1016/j.dental.2014.03.008] [PMID]

[12] Ostrowski N, Roy A, Kumta PN. Magnesium phosphate cement systems for hard tissue applications: A review. ACS Biomaterials Science & Engineering. 2016; 2(7):1067-83. [DOI:10.1021/acsbiomaterials.6b00056] [PMID]

[13] Hesaraki S, Moztarzadeh F, Sharifi D. Formation of interconnected macropores in apatitic calcium phosphate bone cement with the use of an effervescent additive. Journal of Biomedical Materials Research.2007; 83(1):80-7. [DOI:10.1002/jbm.a.31196] [PMID]

[14] Xiong K, Zhang J, Zhu Y, Chen L, Ye J. Zinc doping induced differences in the surface composition, surface morphology and osteogenesis performance of the calcium phosphate cement hydration products. Materials Science & Engineering. C, Materials for Biological Applications. 2019; 105:110065. [DOI:10.1016/j.msec.2019.110065] [PMID]

[15] Graziani V, Fosca M, Egorov AA, Zobkov YV, Fedotov AY, Baranchikov AE, et al. Zinc-releasing calcium phosphate cements for bone substitute materials. Ceramics International. 2016; 42(15):17310-6. [DOI:10.1016/j.ceramint.2016.08.027]

[16] Molenda M, Kolmas J. The role of zinc in bone tissue health and regeneration-a review. Biological Trace Element Research. 2023; 201(12):5640-51. [DOI:10.1007/s12011-023-03631-1] [PMID]

[17] Yamaguchi M. Role of zinc in bone metabolism and preventive effect on bone disorder. Biomedical Research on Trace Elements. 2007; 18(4):346-66. [DOI:10.11299/brte.18.346]

[18] Stiles LI, Ferrao K, Mehta KJ. Role of zinc in health and disease. Clinical and Experimental Medicine. 2024; 24(1):38. [DOI:10.1007/s10238-024-01302-6] [PMID]

[19] Afifi AM, Gordon CR, Pryor LS, Sweeney W, Papay FA, Zins JE. Calcium phosphate cements in skull reconstruction: A meta-analysis. Plastic and Reconstructive Surgery. 2010; 126(4):1300-9. [DOI:10.1097/PRS.0b013e3181ead057] [PMID]

[20] Forouzandeh A, Hesaraki S, Zamanian A. The releasing behavior and in vitro osteoinductive evaluations of dexamethasone-loaded porous calcium phosphate cements. Ceramics International. 2014; 40(1):1081-91. [DOI:10.1016/j.ceramint.2013.06.107]

[21] Struble L. Hydraulic Cements-Physical Properties. Significance of Tests and Properties of Concrete and Concrete-Making Materials. 2006; 169:435. [DOI:10.1520/STP37755S]

[22] Hesaraki S, Nemati R, Nosoudi N. Preparation and characterisation of porous calcium phosphate bone cement as antibiotic carrier. Advances in Applied Ceramics: Structural, Functional and Bioceramics. 2009; 108(4):231-240. [DOI:10.1179/174367608X353656]

[23] Suruagy AA, Alves AT, Sartoretto SC, Calasans-Maia JA, Granjeiro JM, Calasans-Maia MD. Physico-chemical and histomorphometric evaluation of zinc-containing hydroxyapatite in rabbits calvaria. Brazilian Dental Journal. 2016; 27(6):717-26. [DOI:10.1590/0103-6440201601028] [PMID]

[24] Li X, Sogo Y, Ito A, Mutsuzaki H, Ochiai N, Kobayashi T, et al. The optimum zinc content in set calcium phosphate cement for promoting bone formation in vivo. Materials Science & Engineering. C, Materials for Biological Applications. 2009; 29(3):969-75. [DOI:10.1016/j.msec.2008.08.021] [PMID]